MHC Class I Peptides as Chemosensory Signals in the Vomeronasal Organ

Trese Leinders-Zufall,[1] Peter Brennan,[2] Patricia Widmayer,[3] Prashanth Chandramani S.,[3] Andrea Maul-Pavicic,[4] Martina Jäger,[4] Xiao-Hong Li,[1] Heinz Breer,[3] Frank Zufall,[1]* Thomas Boehm[4]*

The mammalian vomeronasal organ detects social information about gender, status, and individuality. The molecular cues carrying this information remain largely unknown. Here, we show that small peptides that serve as ligands for major histocompatibility complex (MHC) class I molecules function also as sensory stimuli for a subset of vomeronasal sensory neurons located in the basal Gαo- and V2R receptor–expressing zone of the vomeronasal epithelium. In behaving mice, the same peptides function as individuality signals underlying mate recognition in the context of pregnancy block. MHC peptides constitute a previously unknown family of chemosensory stimuli by which MHC genotypic diversity can influence social behavior.

The mammalian vomeronasal organ (VNO) is essential for social recognition. Vomeronasal sensory neurons (VSNs) detect pheromones and other chemosignals that carry information about gender, sexual and social status, dominance hierarchies, and individuality, but it has been very difficult to define the molecular nature of these chemosignals (*1*–*13*). The VNO epithelium is segregated into two distinct zones, both of which express a unique set of transduction-related molecules (*2*, *3*, *10*–*12*): (i) an apical (superficial) zone that expresses the G protein Gαi2 as well as members of the V1R family of vomeronasal receptors (~150 genes) and (ii) a basal (deep) zone that characteristically contains VSNs that express Gαo and members of the V2R receptor family (>150 genes). The few molecules that have been identified as sensory stimuli thus far are all small, urine-derived volatiles that activate VSN subpopulations in the apical zone (*4*, *8*, *12*, *13*). Stimuli for VSNs in the basal zone have not yet been found, nor has it been possible to identify any nonvolatile molecules that are widely assumed to be detected by the VSNs (*1*–*3*, *9*, *12*).

We hypothesized that peptide ligands of the major histocompatibility complex (MHC) class I molecules, in addition to their well-established role in the immune system (*14*), may function as sensory stimuli for VSNs. MHC peptides are excellent candidates for social recognition signals that convey information about genetic individuality. The polymorphisms of MHC molecules directly translate into structurally diverse peptide-binding grooves, such that different MHC molecules bind different peptides (*14*). Hence, the structures of peptide ligands mirror the structures of MHC molecules and thus provide a unique molecular signature for each individual. When peptide/MHC complexes are not retained at the cell surface but are instead released into the extracellular space and appear in the urine and other bodily secretions (*15*), any information contained in their chemical complexity becomes a property of the entire individual and potentially can be used for interindividual communication (*16*).

By using an intact VNO preparation to record extracellular field potentials from the microvillous surface of the sensory epithelium (*4*), we tested whether known ligands of MHC class I molecules (*14*) [table S1 and Supporting Online Material (SOM) Text] elicit electrical responses in VSNs of C57BL/6 mice (*17*). These ligands were chosen to correspond to prototypical representatives for two disparate H-2 haplotypes, namely AAPDNRETF (for the H-2^b haplotype of C57BL/6 mice) and SYFPEITHI (for the unrelated H-2^d haplotype of BALB/c mice) (*14*, *18*). Both peptides evoked negative field potentials in a dose-dependent manner in the VNOs of female C57BL/6 mice carrying the H-2^b haplotype, indicating that cognate MHC class I molecules are not required for this response. Threshold responses were observed with concentrations below 10^{-11} M and 10^{-12} M, respectively (Fig. 1, A to D). Control peptides in which the characteristic anchor residues of the two MHC class I ligands were replaced by alanines (i.e., AAPDARETA and SAFPEITHA, respectively) failed to activate VSNs at all concentrations tested (up to 10^{-7} M) (Fig. 1, E and F), indicating that certain structural features of peptides may be required for VSN activation and ruling out an involvement of trace by-products from peptide synthesis

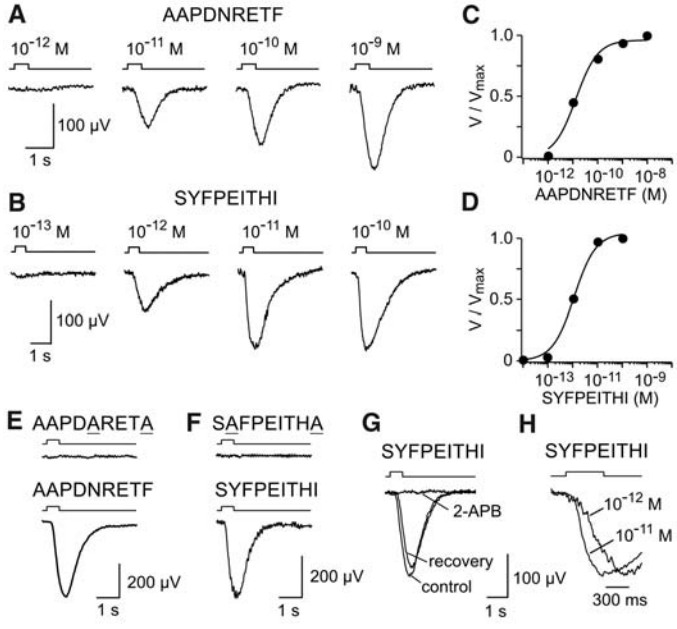

Fig. 1. Class I MHC ligands induce excitatory electrical responses in mouse VNO. (**A** and **B**) Examples of negatively directed field potentials and their dose dependency registered in intact VNO of female C57BL/6 mice. Responses are produced by 500-ms pulses of peptides that were focally ejected from a multibarrelled stimulation pipette. Responses are representative of a total of 17 recordings in six mice. (**C** and **D**) Dose-response plots of peak responses from the two experiments shown in (A) and (B), respectively. Smooth curves are fitted by the Hill equation, with $K_{1/2}$ value and Hill coefficient of 13.3 pM and 0.9 (AAPDNRETF) and 1.2 pM and 1.0 (SYFPEITHI), respectively. (**E** and **F**) Two control peptides (each at 10^{-7} M) failed to elicit an electrical response (n = 13). (**G**) The response to SYFPEITHI and AAPDNRETF (each at 10^{-11} M) is reversibly suppressed by 2-APB (50 µM, n = 3). (**H**) Onset kinetics and initial slope of the rising phase of the field potential depend on stimulus concentration. Responses were scaled to yield the same peak amplitudes.

[1]Department of Anatomy and Neurobiology, University of Maryland School of Medicine, Baltimore, MD 21201, USA. [2]Sub-Department of Animal Behaviour, University of Cambridge, Cambridge CB3 8AA, UK. [3]Institut für Physiologie, Universität Hohenheim, D-70593 Stuttgart, Germany. [4]Department of Developmental Immunology, Max-Planck Institute of Immunobiology, D-79108 Freiburg, Germany.

*To whom correspondence should be addressed. E-mail: boehm@immunbio.mpg.de (T.B.); fzufa001@umaryland.edu (F.Z.)

and purification in the registered responses. Peptide-induced potentials were abolished by 2-aminoethoxydiphenyl borate (2-APB) (50 μM) (Fig. 1G), a blocker of Ca^{2+}-permeable, diacylycerol-gated cation channels essential for VNO transduction, in keeping with results obtained for urine stimuli (*19*).

Next, we investigated the cellular logic underlying peptide recognition and discrimination in the VNO. We first used freshly dissociated VSNs from a transgenic C57BL/6 mouse strain in which all mature VSNs can be visualized on the basis of their expression of green fluorescent protein (GFP) under the control of the regulatory sequences of the *OMP* gene (*20*). VSNs generate an increase in intracellular Ca^{2+} concentration in response to chemostimulation (*4*, *13*, *21*). Cells were loaded with a Ca^{2+} indicator dye, fura-2, and cellular responses were examined optically. Transient somatic Ca^{2+} elevations to peptide stimulations were reproducibly detected in a subset of GFP-positive cells (Fig. 2, A and B). A total of 27 cells responded to stimulation with AAPDNRETF or SYFPEITHI peptides. Of these cells, 10 responded only to the D^b ligand, 15 only to the K^d ligand, and 2 cells responded to both peptides. The response to structurally different peptides is thus specific for individual subsets of VSNs, with only minimal overlap. We then systematically analyzed the spatial representation of peptide responses in large populations of VSNs in the sensory epithelium by using in situ mapping of neuronal activity (*4*). Each peptide produced robust and reproducible increases in intracellular Ca^{2+} in specific subsets of VSNs when tested in such slices (Fig. 2, C to K). In total, we imaged 5183 VSNs (26 slices from 22 mice) of which 85 cells (1.6%) responded to peptide ligands. These signals were reversibly abolished by 2-APB (50 μM) (Fig. 2E), in accord with the field potential recordings of Fig. 1G. Analysis of stimulus-response curves of single VSNs responding to either AAPDNRETF or SYFPEITHI established that these cells are exceptionally sensitive detectors of MHC peptides, with activation thresholds near or below 10^{-12} M. VSNs responding to the same peptide exhibited almost identical dose-response curves (Fig. 2, I and J). The sets of neurons acti-

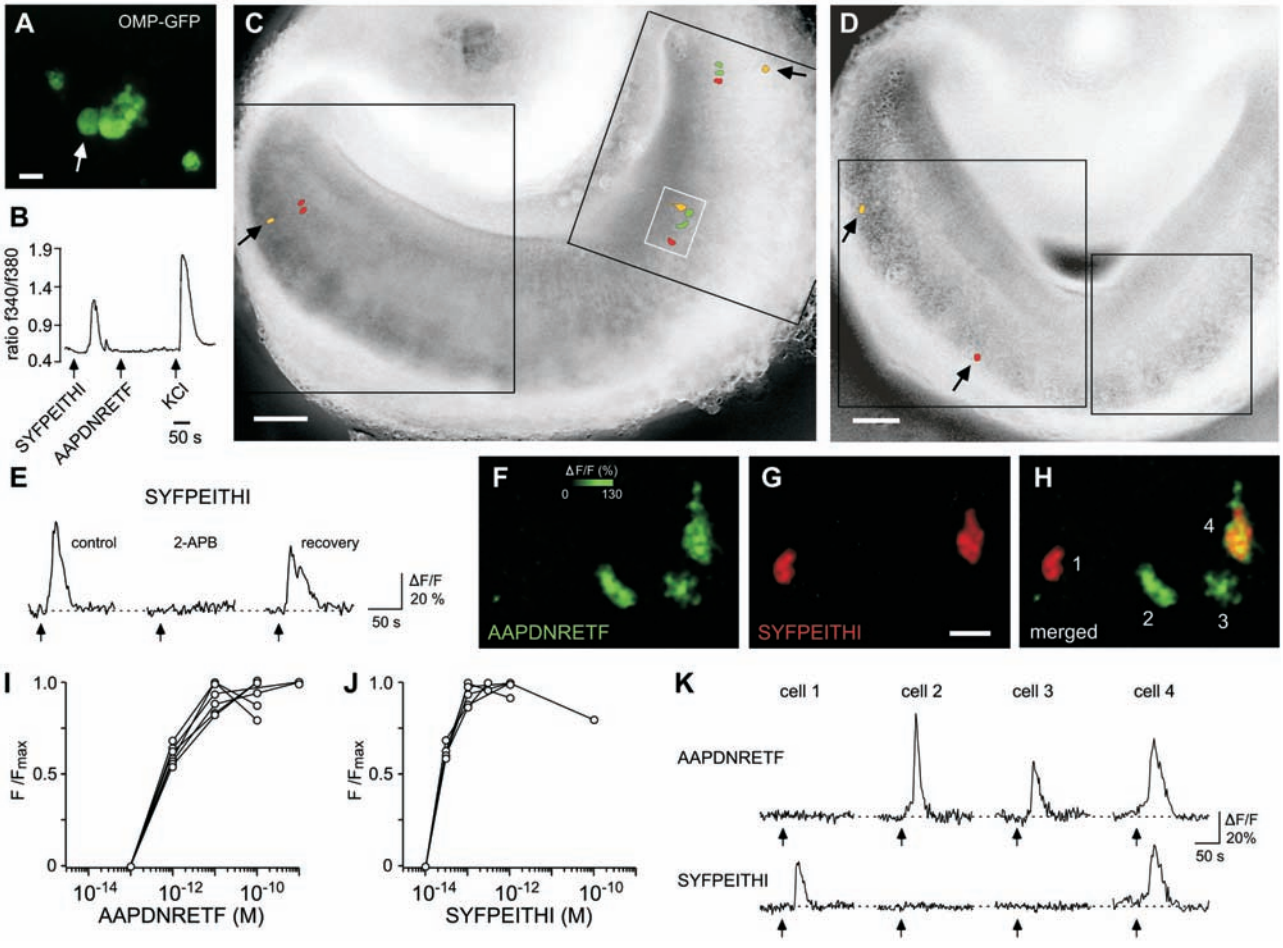

Fig. 2. MHC peptides are detected by distinct populations of VSNs. (**A**) Fluorescence image of freshly dissociated VSNs obtained from an OMP-GFP mouse. White arrow indicates the cell that was analyzed in (B). Scale bar, 10 μm. (**B**) Waveform of somatic Ca^{2+} transients evoked by the application of SYFPEITHI (5×10^{-10} M) or KCl (100 mM). This cell did not respond to AAPDNRETF (5×10^{-10} M). The latencies between stimulus onset and response decrease from left to right because of the design of the perfusion apparatus. (**C** and **D**) Spatial representation of peptide-induced activity in VNO sensory epithelium. Shown are reconstructed VSN response maps ($\Delta F/F$ confocal Ca^{2+} images digitally superimposed onto a transmitted light image of the same slice. F, fluorescence units) for AAPDNRETF (10^{-12} M, green) and SYFPEITHI (10^{-12} M, red). Cells responding to both peptides are color-coded yellow. Black arrows indicate peptide-sensitive VSNs that are localized at the very base of the epithelium. Black boxes, regions that were imaged in these experiments. The white box in (C) is shown at higher magnifications in (F) to (H). Scale bar, 100 μm. (**E**) Ca^{2+} response to SYFPEITHI (10^{-12} M) is reversibly abolished by 2-APB (50 μM, $n = 7$). (**F** to **H**) High-resolution pseudocolor images of the relative increase in peptide-induced Ca^{2+} fluorescence (ratio between the peak fluorescence before and after stimulation, $\Delta F/F$). In this example, AAPDNRETF (10^{-12} M, green) activated three VSNs (cell 2, 3, and 4) and SYFPEITHI (10^{-12} M, red) activated two VSNs (cell 1 and 4). Cell 4 responded to both ligands. Scale bar, 10 μm. Dose-dependency of stimulus-induced Ca^{2+} peak responses of 12 VSNs that recognized either AAPDNRETF (**I**) or SYFPEITHI (**J**). (**K**) Time course of peptide-induced Ca^{2+} responses from the same cells that are depicted in (F) to (H).

vated by structurally different peptides were largely distinct, with only a few cells responding to both peptides (Fig. 2, C, D, F to H, and K). Of 2067 imaged VSNs that were tested with both peptides, 25 (1.2%) responded only to the D^b ligand, 20 (1.0%) only to the K^d ligand, and 8 cells (0.4%) responded to both peptides. To support the physiological relevance of nonvolatile peptides as stimuli of VSNs, we confirmed that nonvolatile stimuli in urine gain access to the vomeronasal epithelium in behaving mice (fig. S1 and SOM Text) and that VSNs activated by synthetic peptides respond also to urine obtained from mice of the relevant haplotype (fig. S2).

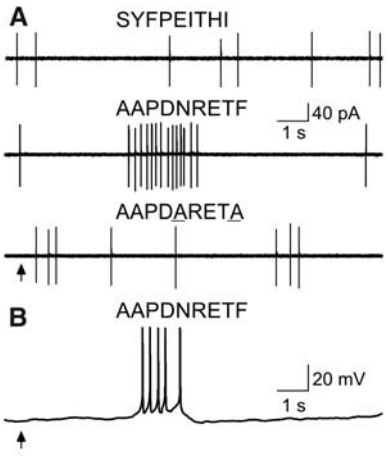

Fig. 3. MHC peptides induce action potential generation in individual VSNs. (**A**) Spontaneous and stimulus-evoked impulse discharges in a VSN after successive application of three different peptides (all at 10^{-11} M). AAPDNRETF, but not SYFPEITHI or AAPDARETA, elicited a transient excitation in this neuron. (**B**) Whole-cell current clamp recording of a VSN that responded to AAPDNRETF (10^{-11} M) with a transient increase in the rate of action potential firing. Resting potential was –62 mV. Arrows indicate the time point at which peptide application was turned on.

Peptides were recognized by sparse populations of VSNs that were widely distributed in the sensory epithelium (Fig. 2, C and D). We noted that activated VSNs were mostly localized to the basal half of the epithelium. Almost one-third of these cells (16/53 or 30%) were found at the very base of the epithelium, close to the basal lamina (Fig. 2, C and D, black arrows). Do peptide-detecting neurons thus belong to those of the basal zone? To address this question, we first identified peptide-sensitive VSNs by in situ Ca^{2+} mapping and then immunostained the tissue with antibodies against Gαo [specific for the basal zone (*2*, *3*, *10*–*12*)] and phosphodiesterase PDE4A [specific for the apical zone (*22*)] (fig. S3A). All 18 peptide-sensitive VSNs were identified as Gαo-positive and PDE4A-negative, irrespective of whether they were located in deep or more superficial regions of the epithelium (fig. S3, B to E). This result was confirmed with dissociated VSNs by using Gαo antibody (*23*). To demonstrate that peptide-sensitive VSNs express V2R receptors, we used an antibody that recognizes the V2R2 receptor, which is broadly expressed in the basal VNO layer (*24*). Double-label immunohistochemistry showed that V2R2 is coexpressed in all Gαo-positive VSNs (fig. S3, F to H). Combining in situ Ca^{2+} mapping and V2R2 immunolabeling, we showed directly that peptide-sensitive VSNs express V2Rs (fig. S3, I to K) (n = 7).

To determine whether peptide stimulation leads to action potential generation in single VSNs, we used the loose-patch technique to register extracellular spike activity from visually identified VSNs in VNO slices (*4*). At 10^{-11} M, the MHC peptides elicited excitatory, sequence-specific responses in a subset of basal VSNs (Fig. 3A) (n = 6), consistent with the Ca^{2+} imaging data. We also used whole-cell current clamp recordings from VSNs in slices (*19*) to demonstrate directly that peptide stimulation produced a membrane depolarization that, in turn, evoked action potential discharges (Fig. 3B) (n = 5).

What are the structural constraints underlying peptide discrimination? We hypothesized that the peptide anchor residues may substantially contribute to the specific recognition by VSNs. Indeed, two different ligands of the K^d MHC molecule, SYFPEITHI and SYIPSAEKI (*14*, *18*), which share the same anchor residues (Y and I) at positions 2 and 9, respectively, but differ substantially in the other positions, activated the same 6 neurons (out of 1109 cells imaged), and their stimulus-response curves were nearly identical (Fig. 4, A to E). VSNs that recognized only one, but not the other, peptide were not observed. The recognition mode of such peptides may thus at least partially resemble that of MHC molecules.

Given that the anchor residues of peptides appear to be essential for VSN activation and that a goldfish V2R-like receptor is known to recognize free amino acids (*25*), it was necessary to rule out that the VSN responses were caused by free amino acids. Isoleucine (10^{-12} M), the C-terminal anchor residue in the K^d peptides, failed to generate a Ca^{2+} signal in five of five cells that detected SYFPEITHI and SYIPSAEKI (Fig. 4D). It also failed to produce a response in 881 other VSNs with unknown tuning properties. Furthermore, in field potential recordings, a mixture containing all amino acids (in free form, each at 10^{-11} M) that constitute the SYIPSAEKI peptide failed to induce any response (Fig. 4F) (n = 11). Likewise, a scram-

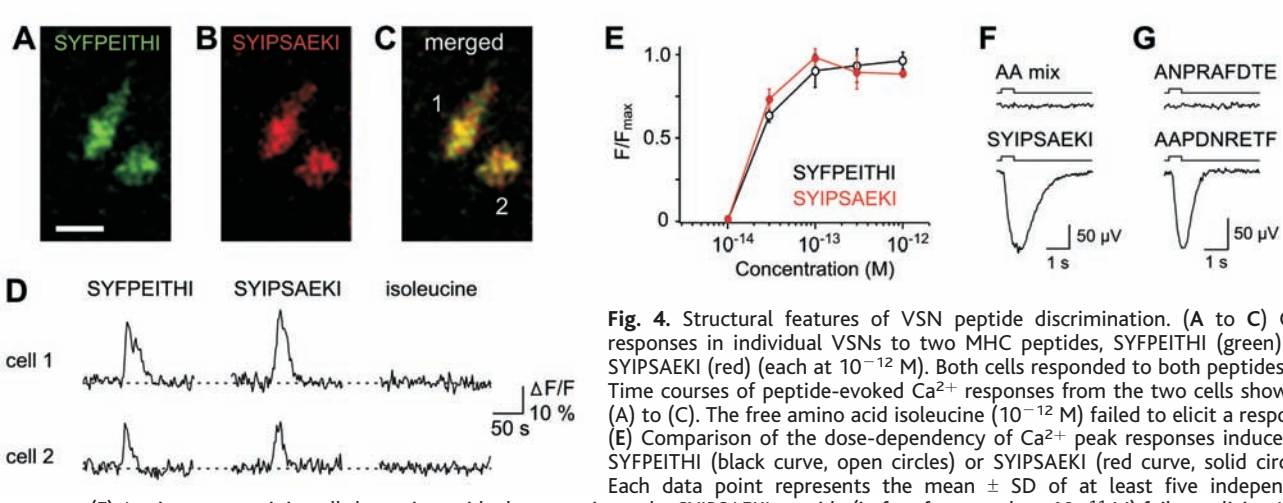

Fig. 4. Structural features of VSN peptide discrimination. (**A** to **C**) Ca^{2+} responses in individual VSNs to two MHC peptides, SYFPEITHI (green) and SYIPSAEKI (red) (each at 10^{-12} M). Both cells responded to both peptides. (**D**) Time courses of peptide-evoked Ca^{2+} responses from the two cells shown in (A) to (C). The free amino acid isoleucine (10^{-12} M) failed to elicit a response. (**E**) Comparison of the dose-dependency of Ca^{2+} peak responses induced by SYFPEITHI (black curve, open circles) or SYIPSAEKI (red curve, solid circles). Each data point represents the mean ± SD of at least five independent measurements. (**F**) A mixture containing all the amino acids that constitute the SYIPSAEKI peptide (in free form, each at 10^{-11} M) fails to elicit a VNO field potential (11 recordings from three mice). (**G**) A scrambled version of the AAPDNRETF peptide, ANPRAFDTE (10^{-11} M), fails to evoke a field potential response (14 recordings from five mice).

bled version of the D^b ligand AAPDNRETF, ANPRAFDTE, failed to evoke any response (Fig. 4G) (n = 14). Thus, peptides must meet precise structural specifications for VSN activation, and peptides of random sequence are unlikely to function as ligands for the receptors on VSNs.

Given that MHC peptides activate VSNs in a sequence-specific manner, they could potentially function as individuality signals during social recognition. In mice, selective pregnancy failure [the Bruce effect (*26*)] represents an excellent paradigm to assess this hypothesis in vivo, because it depends critically on signaling via the accessory olfactory system (SOM Text) and requires the capacity to differentiate between individuality cues (*27*). Female mice of the BALB/c inbred strain (H-2^d haplotype) were mated with BALB/c males and then exposed to urine taken from either a BALB/c male (mating male urine) or C57BL/6 male (unfamiliar male urine; H-2^b haplotype). Application of the unfamiliar urine, coincident with the postmating peaks in prolactin levels, reliably resulted in a high level of pregnancy failure, whereas the familiar urine did not (Fig. 5, experiments 1 and 2). When BALB/c females were mated with C57BL/6 males, pregnancy block occurred after the application of BALB/c urine, but not of C57BL/6 urine (Fig. 5, experiments 3 and 4), establishing the strain specificity of pregnancy block (*28*). To test whether familiar male urine could be converted to unfamiliar urine, we added peptides of disparate H-2 haplotype specificity. Exposure of BALB/c-mated BALB/c females to a mixture of H-2^b class I peptides in BALB/c mating male urine was equally effective as C57BL/6 urine (Fig. 5, experiment 6). The addition of a mixture of H-2^d peptides had no effect (Fig. 5, experiment 5). Conversely, exposure of C57BL/6-mated BALB/c females to BALB/c peptides in C57BL/6 mating male urine was effective at blocking pregnancy; here, C57BL/6 peptides were ineffective. Experiments 5 to 8 show that peptides per se do not cause pregnancy failure and that this function depends on the previous mating combination. The overall occurrence of pregnancy block upon exposure to the strange male H-2 peptides of 64% (n = 47; combined results of experiments 6 and 7) was significantly higher than the 25% (n = 24; combined results of experiments 5 and 8) elicited by exposure to mating male H-2 peptides (P = 0.002, Fisher exact probability test).

Our experiments identified an unexpected role for MHC class I peptides as chemosensory stimuli. MHC class I ligands are recognized by VSNs in the basal layer of the VNO. Recognition of peptides by VSNs is independent of MHC haplotype, and peptides specific for different MHC molecules (i.e., carrying different anchor residues) generate unique VSN activation patterns, providing the basis for the neural representation of the structural diversity of this new family of chemosignals.

Our data demonstrate that the VNO can detect both nonvolatile and volatile stimuli, a result that is fully compatible with early predictions (*29*). Peptide responses were found exclusively in Gαo- and V2R-positive neurons, whereas responses to volatile stimuli have been mapped to the apical V1R-expressing zone (*4*). Whether this functional segregation is true for all vomeronasal stimuli remains to be seen. V2R receptors constitute a large family of orphan receptors (*2*, *3*, *10*–*12*) that differ from V1Rs and olfactory receptors by the presence of a large N-terminal domain. They are coexpressed with MHC class Ib molecules at the cell surface of VSNs (*30*, *31*). MHC class Ib molecules can bind peptides, but they lack the typical peptide-binding groove and specificity of classical MHC class I molecules (*32*). Sequence-specific recognition of peptides may thus be achieved by the N-terminal domain of certain V2R receptors (or receptor combinations), whereas the MHC class Ib molecules may serve as a general presentation device. Given the limited diversity of amino acid residues occupying the two anchor positions of mouse MHC class I peptides (*14*), we estimate that about 50 different receptors should be sufficient to discriminate ligands from all known mouse MHC class I molecules.

Considerable work has focused on the main olfactory system in the detection of MHC-related odor signals (*33*, *34*). Our results highlight the role of the VNO in this process but do not preclude a role of the main olfactory system in individual recognition, nor do they preclude a role for other molecules such as volatile urinary constituents (*34*) or polymorphic major urinary proteins (*35*). MHC peptides may thus form one class of different signals that may be used in different behavioral contexts. For a meaningful biological response to occur in MHC-related behaviors, signals about gender, reproductive status, and species identity must be evaluated alongside signals of genetic individuality, and this may involve remotely sensed signals as well as signals that are detected during direct contact. A chemosensory function of MHC peptides provides a direct link between MHC diversity and MHC-related behavior, converting a MHC genotype into an olfactorily detectable quality.

Experiment	1	2	3	4	5	6	7	8
Mating exposure								
BALB/c	+	+	-	-	+	+	-	-
C57BL/6	-	-	+	+	-	-	+	+
Stimulus exposure								
BALB/c urine	+	-	+	-	+	+	-	-
C57BL/6 urine	-	+	-	+	-	-	+	+
BALB/c peptides	-	-	-	-	+	-	+	-
C57BL/6 peptides	-	-	-	-	-	+	-	+

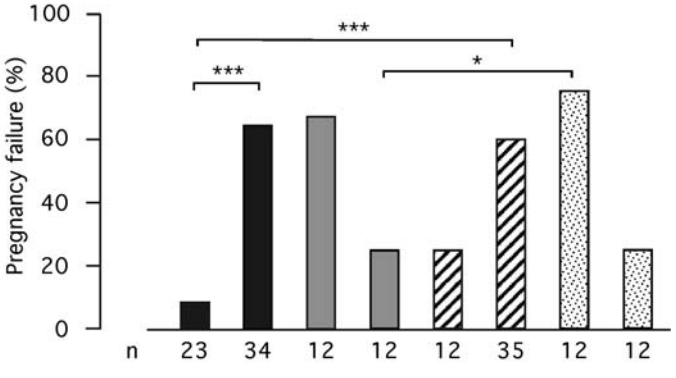

Fig. 5. Peptides function as individuality signals in the context of pregnancy block. Percent pregnancy failure in female BALB/c (H-2^d haplotype) mice mated with either BALB/c (H-2^d haplotype) or C57BL/6 (H-2^b haplotype) males as indicated (+). Exposure to different male urine types, which, in some cases, were supplemented with peptides specific for BALB/c or C57BL/6 haplotypes, is indicated. *P < 0.05; ***P < 0.001 (Fisher exact probability test with Bonferroni correction for multiple comparisons).

References and Notes

1. C. J. Wysocki, M. Meredith, in *Neurobiology of Taste and Smell*, T. E. Finger, W. L. Silver, Eds. (Wiley, New York, 1987), pp. 125–150.
2. R. Tirindelli, C. Mucignat-Caretta, N. J. Ryba, *Trends Neurosci.* **21**, 482 (1998).
3. P. A. Brennan, E. B. Keverne, *Curr. Biol.* **14**, R81 (2004).
4. T. Leinders-Zufall *et al.*, *Nature* **405**, 792 (2000).
5. T. E. Holy, C. Dulac, C. M. Meister, *Science* **289**, 1569 (2000).
6. L. Stowers, T. E. Holy, M. Meister, C. Dulac, G. Koentges, *Science* **295**, 1493 (2002); published online 31 January 2002 (10.1126/science.1069259).
7. B. G. Leypold *et al.*, *Proc. Natl. Acad. Sci. U.S.A.* **99**, 6376 (2002).
8. K. Del Punta *et al.*, *Nature* **419**, 70 (2002).
9. M. Luo, M. S. Fee, L. C. Katz, *Science* **299**, 1196 (2003).
10. C. I. Bargmann, *Cell* **90**, 585 (1997).
11. C. Dulac, A. T. Torello, *Nature Rev. Neurosci.* **4**, 551 (2003).
12. P. Mombaerts, *Nature Rev. Neurosci.* **5**, 263 (2004).
13. C. Boschat *et al.*, *Nature Neurosci.* **5**, 1261 (2002).
14. H. G. Rammensee, J. Bachmann, S. Stefanovic, *MHC*

Ligands and Peptide Motifs (Landes Bioscience, Georgetown, TX, 1997).
15. P. B. Singh, R. E. Brown, B. Roser, *Nature* **327**, 161 (1987).
16. T. Boehm, C. C. Bleul, M. Schorpp, *Immunol. Rev.* **195**, 15 (2003).
17. Materials and methods are available as supporting material on *Science* Online.
18. Single-letter abbreviations for the amino acid residues are as follows: A, Ala; C, Cys; D, Asp; E, Glu; F, Phe; G, Gly; H, His; I, Ile; K, Lys; L, Leu; M, Met; N, Asn; P, Pro; Q, Gln; R, Arg; S, Ser; T, Thr; V, Val; W, Trp; and Y, Tyr.
19. P. Lucas, K. Ukhanov, T. Leinders-Zufall, F. Zufall, *Neuron* **40**, 551 (2003).
20. S. M. Potter *et al.*, *J. Neurosci.* **21**, 9713 (2001).
21. M. Spehr, H. Hatt, C. H. Wetzel, *J. Neurosci.* **22**, 8429 (2002).
22. Y. E. Lau, J. A. Cherry, *Neuroreport* **11**, 27 (2000).
23. T. Leinders-Zufall *et al.*, data not shown.
24. S. Martini, L. Silvotti, A. Shirazi, N. J. Ryba, R. Tirindelli, *J. Neurosci.* **21**, 843 (2001).
25. D. J. Speca *et al.*, *Neuron* **23**, 487 (1999).
26. H. M. Bruce, *Nature* **184**, 105 (1959).
27. A. Lloyd-Thomas, E. B. Keverne, *Neuroscience* **7**, 907 (1982).
28. The efficiency of pregnancy block by direct application of unfamiliar urine is similar to that caused by the presence of unfamiliar mice (for instance, when BALB/c females are mated with C57BL/6 males, presence of BALB/c males causes pregnancy failure in 9 of 12 mice).
29. R. J. O'Connell, M. Meredith, *Behav. Neurosci.* **98**, 1083 (1984).
30. T. Ishii, J. Hirota, P. Mombaerts, *Curr. Biol.* **13**, 394 (2003).
31. J. Loconto *et al.*, *Cell* **112**, 607 (2003).
32. X. L. He, P. Tabaczewski, J. Ho, I. Stroynowski, K. C. Garcia, *Structure* **9**, 1213 (2001).
33. D. Penn, W. Potts, *Adv. Immunol.* **69**, 411 (1998).
34. G. K. Beauchamp, K. Yamazaki, *Biochem. Soc. Trans.* **31**, 147 (2003).
35. J. L. Hurst *et al.*, *Nature* **414**, 631 (2001).

36. We thank R. Escher for peptide synthesis, J. Cherry for PDE4A antibodies, R. Tirindelli for V2R2 antibodies, P. Mombaerts for OMP-GFP mice, and K. Kelliher for the demonstration that nonvolatile chemicals can reach the VNO in vivo. This work was supported by the Leibniz program of the Deutsche Forschungsgemeinschaft (T.B. and H.B.), by NIH/National Institute on Deafness and other Communication Disorders (T.L.-Z. and F.Z.), and by the Hochshul- und Wissenschafts-Programm (P.W.).

Supporting Online Material

www.sciencemag.org/cgi/content/full/306/5698/1033/DC1
Materials and Methods
SOM Text
Figs. S1 to S4
Table S1
References

15 July 2004; accepted 9 September 2004

Autophagy Defends Cells Against Invading Group A *Streptococcus*

Ichiro Nakagawa,[1,3]* Atsuo Amano,[2,4] Noboru Mizushima,[3,5] Akitsugu Yamamoto,[6] Hitomi Yamaguchi,[7] Takahiro Kamimoto,[7] Atsuki Nara,[6,7] Junko Funao,[1] Masanobu Nakata,[1] Kayoko Tsuda,[7] Shigeyuki Hamada,[1] Tamotsu Yoshimori[4,7]*

We found that the autophagic machinery could effectively eliminate pathogenic group A *Streptococcus* (GAS) within nonphagocytic cells. After escaping from endosomes into the cytoplasm, GAS became enveloped by autophagosome-like compartments and were killed upon fusion of these compartments with lysosomes. In autophagy-deficient Atg5$^{-/-}$ cells, GAS survived, multiplied, and were released from the cells. Thus, the autophagic machinery can act as an innate defense system against invading pathogens.

Autophagy mediates the bulk degradation of cytoplasmic components in eukaryotic cells in which a portion of the cytoplasm is sequestered in an autophagosome and eventually degraded upon fusion with lysosomes (*1*–*3*). *Streptococcus pyogenes* (also known as group A *Streptococcus*, GAS) is the etiological agent for a diverse collection of human diseases (*4*). GAS invades nonphagocytic cells (*5*, *6*), but the destination of GAS after internalization is not well understood. To clarify the intracellular fate of GAS, especially any possible involvement of autophagy, we first investigated whether intracellular GAS colocalizes with LC3, an autophagosome-specific membrane marker, following invasion of HeLa cells (*7*–*9*). After infection, GAS strain JRS4 cells colocalized with LC3-positive vacuole-like structures in HeLa cells (Fig. 1A). The size (5 to 10 μm) and morphology of the structures were distinct from standard starvation-induced autophagosomes with a diameter of about 1 μm (fig. S1A), so we designated these structures GAS-containing LC3-positive autophagosome-like vacuoles (GcAVs). The number of cells bearing GcAVs, the area of GcAVs, and ratio of GAS trapped in GcAVs to total intracellular GAS increased in a time-dependent manner, reaching a maximum at 3 hours after infection (Fig. 1, B and C; figs. S1B and S2A). A similar result was obtained in mouse embryonic stem (ES) cells (figs. S2B and S3A). About 80% of intracellular GAS were eventually trapped by the compartments (Fig. 1C; fig. S1B). LC3 frequently surrounded GAS, fitting closely around a GAS chain (Fig. 1, D and E; movie S1).

LC3 exists in two molecular forms. LC3-I (18 kD) is cytosolic, whereas LC3-II (16 kD) binds to autophagosomes (*7*, *8*). The amount of LC3-II, which directly correlates with the number of autophagosomes (*8*), increased after infection (Fig. 1F). Thus, GAS invasion appears to induce autophagy, specifically trapping intracellular GAS.

To substantiate this idea, we examined GcAV formation in Atg5-deficient (Atg5$^{-/-}$) cells lacking autophagosome formation (*7*). In contrast to the wild-type cells (fig. S2, B and C), no GcAVs were observed in Atg5$^{-/-}$ ES cells (J1-2) (Fig. 2A) or in Atg5$^{-/-}$ mouse embryonic fibroblasts (MEFs) (fig. S2C). Thus, GcAV formation requires an Atg5-mediated mechanism. We also examined LC3-II formation. During infection with GAS, Atg5$^{-/-}$ cells showed no induction of LC3-II (Fig. 2B). By electron microscopy, in wild-type MEF cells infected with GAS, we observed characteristic cisternae surrounding GAS in the cytoplasm (Fig. 2C). No GAS were found surrounded by the membranes in Atg5$^{-/-}$ cells (Fig. 2C). The autophagosome-like multiple membrane–bound compartment containing GAS was also found in HeLa cells (Fig. 2D).

Next, we asked whether the bacteria are killed or survive after entering the compartments. To address this question, we directly scored bacterial viability by counting colony-forming units (CFU viability assay) in wild-type and Atg5$^{-/-}$ MEFs (Fig. 2E). In wild-type MEFs at 4 hours after infection, intracellular GAS had been killed (Fig. 2E), whereas the decrease of GAS viability was suppressed in the Atg5$^{-/-}$ MEFs. Tannic acid is a cell-impermeable fixative that prevents fusion between secretory vesicles and the plasma membrane but does not affect intracellular membrane trafficking (*10*). In Atg5$^{-/-}$ cells treated with tannic acid to prevent external escape of GAS, the viable bacteria increased by 2 hours after infection and maintained this level at 4 hours after infection (Fig. 2E). In contrast, the numbers of intracellular GAS decreased rapidly in tannic acid–treated wild-type cells as well

[1]Department of Oral and Molecular Microbiology, [2]Department of Oral Frontier Biology, Osaka University Graduate School of Dentistry, 1-8 Yamadaoka, Suita-Osaka 565-0871, Japan. [3]PRESTO, [4]CREST, Japan Science and Technology Agency, Kawaguchi-Saitama 332-0012, Japan. [5]Department of Bioregulation and Metabolism, The Tokyo Metropolitan Institute of Medical Science, 3-18-22 Honkomagome, Bunkyo-ku, Tokyo 113-8613, Japan. [6]Department of Cell Biology, Faculty of Bio-Science, Nagahama Institute of Bio-Science and Technology, 1266 Tamura-cho, Nagahama-Shiga 526-0829, Japan. [7]Department of Cell Genetics, National Institute of Genetics/SOKENDAI, Yata 1111, Mishima-Shizuoka 411-8540, Japan.

*To whom correspondence should be addressed. E-mail: ichiro@dent.osaka-u.ac.jp and tamyoshi@lab.nig.ac.jp